**Atmospheric
Chemistry
and Physics**

Optical and physical properties of aerosols in the boundary layer and free troposphere over the Amazon Basin during the biomass burning season

D. Chand[1,*], **P. Guyon**[1], **P. Artaxo**[2], **O. Schmid**[1,**], **G. P. Frank**[1], **L. V. Rizzo**[2], **O. L. Mayol-Bracero**[3], **L. V. Gatti**[4], and **M. O. Andreae**[1]

[1]Max Planck Institute for Chemistry, Mainz, Germany
[2]Institute of Physics, University of São Paulo, São Paulo, Brazil
[3]University of Puerto Rico, San Juan, PR, USA
[4]Institute of Nuclear Energy Research, São Paulo, Brazil
[*]now at: University of Washington-Bothell, Bothell, USA
[**]now at: GSF-Research Center for Environment and Health, Neuherberg/Munich, Germany

Abstract. As part of the Large Scale Biosphere-Atmosphere Experiment in Amazonia – Smoke, Aerosols, Clouds, Rainfall and Climate (LBA-SMOCC) campaign, detailed surface and airborne aerosol measurements were performed over the Amazon Basin during the dry to wet season from 16 September to 14 November 2002. Optical and physical properties of aerosols at the surface, and in the boundary layer (BL) and free troposphere (FT) during the dry season are discussed in this article. Carbon monoxide (CO) is used as a tracer for biomass burning emissions. At the surface, good correlation among the light scattering coefficient (σ_s at 545 nm), PM2.5, and CO indicates that biomass burning is the main source of aerosols. Accumulation of haze during some of the large-scale biomass burning events led to high PM2.5 (225 μg m^{-3}), σ_s (1435 Mm^{-1}), aerosol optical depth at 500 nm (3.0), and CO (3000 ppb). A few rainy episodes reduced the PM2.5, number concentration (CN) and CO concentration by two orders of magnitude. The correlation analysis between σ_s and aerosol optical thickness shows that most of the optically active aerosols are confined to a layer with a scale height of 1617 m during the burning season. This is confirmed by aircraft profiles. The average mass scattering and absorption efficiencies (545 nm) for small particles (diameter D_p<1.5 μm) at surface level are found to be 5.0 and 0.33 m^2 g^{-1}, respectively, when relating the aerosol optical properties to PM2.5 aerosols. The observed mean single scattering albedo (ω_o at 545 nm) for submicron aerosols at the surface is 0.92±0.02. The light scattering by particles ($\Delta\sigma_s/\Delta$CN) increase 2–10 times from the surface to the FT, most probably due to the combined affects of coagulation and condensation.

---

1 Introduction

The gas and particle emissions from tropical biomass burning influence the physical, chemical and optical properties of the atmosphere (Andreae et al., 1988, 2002; Crutzen and Andreae, 1990; Andreae and Crutzen, 1997; Hobbs et al., 1997, 2003; Artaxo et al., 1998, 2001, 2002; Andreae and Merlet, 2001, Ramanathan et al., 2001). Smoke aerosols contain a significant amount of partially oxidized organic material and black carbon or soot, which may have significant climatic implications (IPCC, 2001). Aerosol particles interact directly with the incoming solar radiation by the scattering and absorption of light (Charlson et al., 1992; Rosenfeld, 2000; Andreae et al., 2004) and because they act as cloud condensation nuclei (CCN), thereby affecting indirectly the Earth's radiation budget. The importance of aerosol particles for climate forcing is recognized, but the magnitude of their contribution is highly uncertain (IPCC, 2001). It is thought that particles, through their combined direct and indirect effects, may currently have an influence of potentially similar magnitude, but opposite sign, as greenhouse gas forcing (IPCC, 2001). Aerosol radiative forcing may range from net heating to net cooling, depending on the aerosol properties as well as on the albedo of the boundary layer and free troposphere aerosols. Particles, with their short atmospheric lifetimes, have significant vertical, horizontal and temporal

Correspondence to: D. Chand
(duli@mpch-mainz.mpg.de)

concentration gradients. These spatial gradients correspond to significant local/regional as well as global aerosol forcing effects. For example, smoke layers over the Amazon basin can have significant regional effects by reduction of regional photosynthetically active radiation up to 45% (Eck et al., 1998). Because of their light absorbing properties, the presence of aerosol particles can result in the radiative forcing at the surface being much larger than at the top of the atmosphere (Satheesh and Ramanathan, 2000; Ramanathan et al., 2001; Procópio et al., 2003, 2004).

Biomass burning, particularly in the tropics, is a major source of atmospheric trace gases and particles (Andreae and Merlet, 2001). Being the world's largest rain forest area containing approximately one quarter of all tropical rainforests, the Amazon Basin is subject to one of the highest rates of deforestation in the world (Gash et al., 1996). About 80% of the global burning activity is taking place in the tropics and one third of it occurs in South America alone. Under suitable meteorological conditions, the local chemical, physical, and optical characteristics of aerosols can be much different from the global or regional averages and these characteristics, in turn, are strongly influenced by local and regional sources and perturbations, e.g., forest emissions, fires, dust, sea salt, etc., leading to further spatial and temporal inhomogeneity.

Aerosol optical properties over the Amazon Basin have been studied in the previous LBA and SCAR-B experiments (e.g., Eck et al., 1998, 2003; Kotchenruther and Hobbs, 1998; Martins et al., 1998; Reid et al., 1998; Reid and Hobbs, 1998; Ross et al., 1998, Guyon et al., 2003a, 2004; Reid et al., 2005a, b). In these studies, the variability in aerosol optical properties has been analyzed based on either surface or airborne measurements. However, so far, it is not understood how aerosol properties at the surface relate to those aloft in the boundary layer (BL)[1] and free troposphere. In addition to the limited surface observations, only a few series of in-situ vertical profile measurements of aerosol optical properties (e.g., light absorption, light scattering, hemispheric backscattering) have been made over the Amazon Basin (e.g., Kotchenruther and Hobbs, 1998; Reid et al., 1998, 2005a, b; Ross et al., 1998; Guyon et al., 2003a, c). To our knowledge, almost no simultaneous observations of optical properties of aerosols and trace gases at the surface and aloft are available over the Amazon Basin in the biomass burning season.

This paper describes the vertical distribution of aerosol optical and physical properties over the Amazon Basin during the 2002 biomass burning season. The observations of light scattering (σ_s), light absorption (σ_a), aerosol optical thickness (AOT), aerosol number density (CN), aerosol mass concentration (PM2.5), and carbon monoxide (CO) are being used to address the following scientific questions: (1) How does σ_s vary at the surface, in the boundary layer and free tro-

posphere? (2) How does σ_s vary vertically at different sites over the Amazon Basin? (3) How do Ångström exponent observations from the airborne measurements compare with vertically integrated measurements using a sunphotometer?

2 Instrumentation and methods

2.1 Observational sites

The measurements were made over the Amazon Basin during the Large Scale Biosphere-Atmosphere Experiment in Amazonia – Smoke, Aerosols, Clouds, Rainfall and Climate (LBA-SMOCC) from 16 September to 14 November in 2002. Detailed surface observations of aerosols and trace gases were made in the state of Rondônia, Brazil at a pasture site "Fazenda Nossa Senhora Aparecida" (10.76° S, 62.32° W, 315 m above mean sea level (a.m.s.l.)), hereafter FNS. This experimental site is located about 57 km north-west of the town of Ji-Paraná (10.88° S, 61.85° W, 235 m a.m.s.l.). A few small hills (300–400 m a.m.s.l.) are located about 1–4 km from FNS. One hill, known as "Abracos Hill", is one of the AERONET (Aerosol Robotic Network) sites and provides column integrated aerosol optical thickness (AOT) measurements using sun-photometry observations (Holben et al., 1998). Further details on the FNS site can be found elsewhere (Kirkman et al., 2002; Trebs et al., 2004). Airborne measurements in the BL and free troposphere (FT, up to 4200 m) over the Amazon Basin were taken as far as 800 km from FNS. Some selected flight tracks along with the geographical location of the surface measurement site FNS are shown in Fig. 1. More details on this campaign are given in Andreae et al. (2004).

2.2 Measurements and methods

The surface observations at FNS over the Amazon basin were conducted from the middle of the smoky dry season (16 September) to the onset of the wet season (14 November), when pollution levels approached background conditions. In this study, we make use of ground based observations from 16 September to 8 October representing the biomass burning season during the SMOCC campaign.

Aerosol mass (PM2.5) and σ_s measurements at FNS were made using dried air (*RH*<40%) sampled from an inlet installed at about 10 m above the ground level. The hygroscopic growth in scattering coefficient at *RH* 30–50% is low (<10%) for the observed submicron aerosols (<1.5 μm). The details of the measured parameters are given in Table 1. The σ_s and σ_a of dried aerosols at FNS were measured for the submicron size particles. An impactor with a cut off diameter at 1.5 μm was used to remove the bigger particles (Table 2). Before selection through the impactor, the aerosols were dried by passing them through a Permapure Nafion drier. The drier unit and impactor (with and without impaction plate) were characterized for aerosol losses using

---

[1] Boundary layer (BL) is the lowest layer of the atmosphere near ground affected by diurnal heat, moisture or momentum transfer to or from the surface.

Table 1. Summary of the optical and physical properties of aerosols along with CO concentration at surface (S), boundary layer (BL) and free troposphere (FT) during the biomass burning season. The availability of measurements at S, BL and FT are shown by right ($\sqrt{}$) sign and the "x" shows the parameters with no observations.

Parameter with units	Symbols	Measurements		
		S	BL	FT
Light scattering coefficient at 545, 550 nm (Mm^{-1})	σ_s	$\sqrt{}$	$\sqrt{}$	$\sqrt{}$
Light absorption coefficient at 532 nm (Mm^{-1})	σ_a	$\sqrt{}$	x	x
Condensation nuclei (cm^{-3})	CN	$\sqrt{}$	$\sqrt{}$	$\sqrt{}$
Aerosol mass ($g\,cm^{-3}$)	PM2.5	$\sqrt{}$	x	x
Aerosols optical thickness at 440, 670 nm	AOT	Column integrated		
Carbon monoxide (ppb)	CO	$\sqrt{}$	$\sqrt{}$	$\sqrt{}$
Single scattering albedo (using σ_s and σ_a) at 545 nm*	ω_o	$\sqrt{}$	x	x
Excess ratio ($\Delta\sigma_s/\Delta CN$)	$\Delta\sigma_s/\Delta CN$	$\sqrt{}$	$\sqrt{}$	$\sqrt{}$
Excess ratio ($\Delta\sigma_s/\Delta CO$)	$\Delta\sigma_s/\Delta CO$	$\sqrt{}$	$\sqrt{}$	$\sqrt{}$
Excess ratio ($\Delta\sigma_s/\Delta PM2.5$) or Mass scattering efficiency ($m^2\,g^{-1}$)*	$\Delta\sigma_s/\Delta PM2.5$	$\sqrt{}$	x	x
Excess ratio ($\Delta\sigma_a/\Delta PM2.5$) or Mass absorption efficiency ($m^2\,g^{-1}$)*	$\Delta\sigma_a/\Delta PM2.5$	$\sqrt{}$	x	x

* To match σ_s wavelength, the σ_a observation at 532 nm are converted to 545 nm. The calculated ω_o, σ_a and σ_s are presented at 545 nm

Table 2. The size cut-point (aerodynamic diameter) of the aerosols property is given by D_{p-cut}.

Aerosol parameter	Dry/Ambient	Symbol	D_{p-cut}
Light scattering coefficient (545 nm) at ground (FNS)	(D)	σ_s	$1.5\,\mu m$
Light scattering coefficient (550 nm) in BL (aircraft)	(A)	σ_s	–
Light absorption coefficient at 532 nm*	(D)	σ_a	$1.5\,\mu m$
Condensation nuclei (cm^{-3})	(A)	CN	–
Aerosols optical thickness at 440, 670 nm	(A)	AOT	–
Particulate mass	(A)	PM2.5	$2.5\,\mu m$
Single scattering albedo for FNS observations	(D)	ω_o	$1.5\,\mu m$
Mass absorption efficiency ($m^2\,g^{-1}$)	(D)	α_a	$1.5\,\mu m^{\dagger}$
Mass scattering efficiency ($m^2\,g^{-1}$)	(D)	α_s	$1.5\,\mu m^{\dagger}$

* To match the σ_s wavelength, the σ_a observation at 532 nm are converted to 545 nm
† based on correlations of σ_s and σ_a with PM2.5; (A) Ambient aerosol; (D) Dry aerosol

ammonium sulfate particles in the lab at the same flows as used in the field campaign. We used a series of lab experiments to characterize the losses in the impactor and Nafion drier. First, dried particles of the desired diameter were selected using the SMPS, and then these size-selected aerosols were counted before and after passing through the Nafion tube. Similar experiments were conducted using the combined (Nafion+impactor) units. To avoid particle losses in the lines, smooth bends were used and the flow was optimized. Most of the losses are confined to very small sizes (diameter<60 nm) that have very little effect on the measured σ_s and σ_a. Using Mie theory and the measured on-site particle size distributions we found a 2–4% reduction in σ_s and σ_a during the burning season. All the σ_s and σ_a data sets at FNS were corrected for these losses. Non-lambertian correction on σ_s is applied for dried aerosols as per Anderson and Ogren (1998). The radiance research (RR) nephelome-

ter, photoacoustic spectrometer (PAS) and particle soot absorption photometer (PSAP) were operating downstream of the impactor-drier units, and the losses observed by these instruments were of the same order.

Airborne measurements of aerosols and trace gases were made from 25 September to 19 October (about 31 flights). For this study, we make use of the airborne measurements of σ_s, aerosol number density (CN), limited available size distribution (diameter, D_p=42–346 nm) and carbon monoxide (CO) from selected flights (numbers 4, 6, 7, 8 and 24), which include measurements conducted directly above FNS and its surroundings. A Scanning Mobility Particle Sizer (SMPS, TSI Model 3080) was used to measure the diameter of the submicron aerosols during the airborne observations. The flight tracks of these observations along with dates are shown in Fig. 1 with complementary data in Table 3. Most of the flights were conducted during afternoon
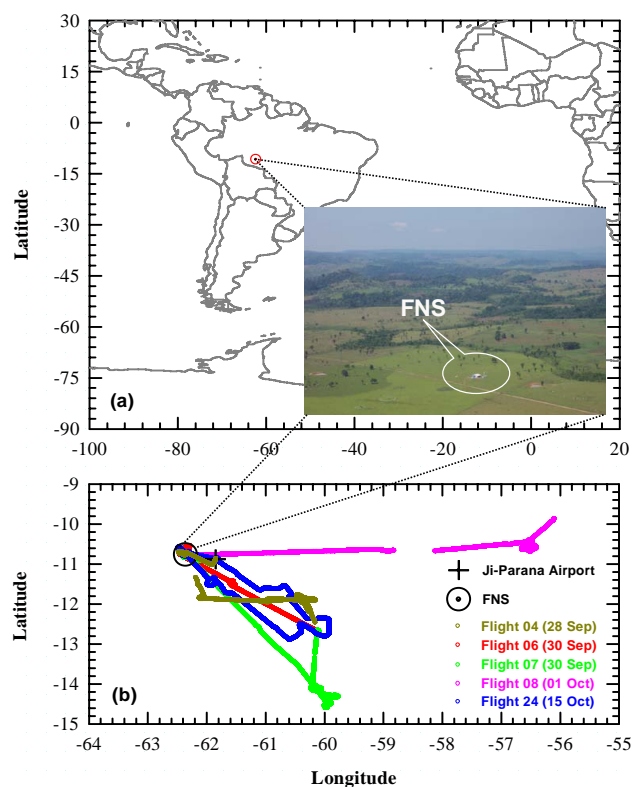
Fig. 1. (a) Overview map showing the geographical location of the surface site FNS. The picture is an aerial view of the site. **(b)** Flight tracks for flights 4, 6, 7, 8, and 24. The positions of FNS and the nearby Ji-Paraná airport are shown by the circle and cross symbols, respectively.

hours (14:00 LT=18:00 UT) when the BL was well developed. Flights 6 and 7 were conducted on the same day during morning and afternoon hours, respectively. The measurements were taken up to a height of 4200 m. The time schedule of the studied parameters, their symbols, and further details on the surface and airborne observations are given in Tables 1–4. Some other details on the aircraft measurements can be found in Guyon et al. (2005).

The time resolution of the σ_s and σ_a measurements at FNS was one minute; they were averaged over longer intervals (30 min) to match the averaging time of the aerosol mass (PM2.5) measurement. A real-time aerosol mass monitor, the Tapered Element Oscillating Microbalance (TEOM, series 1400a, Rupprecht & Patashnick Inc.) was used to measure PM2.5 aerosol mass concentration with a time resolution of 30 min. The TEOM inlet was heated to 50°C for drying the aerosols. The aerosol number density was measured using a TSI condensation particle/nuclei (CN) counter (model 3022A) with a minimum detection size of 8 nm. At the ground site CO was measured with the Thermo Environmental Instrument Inc. analyzer (Model 48C Gas Filter Correlation) with a minimum detection limit of 40 ppb. Because

of the high ambient humidity, a cooler was used to remove water from the sample stream prior to the CO analyzer. The CO measurements on the aircraft were made using an Aero-Laser (AL5002) instrument operating at 1 Hz. Prior to sampling, the air was dried using a Nafion drier in the CO instrument. The CO, σ_s and CN were measured both at the ground site and on the aircraft. The airborne observations are compared with measurement at FNS during fly-by over FNS at height of 150–600 m. These data (1–3 min every flight) were used to compare the observations at surface and aloft. The CN are found higher in the airborne observations by 5–10% compared to FNS. Also, the ratios of the σ_s and CO from airborne observation were higher compared to FNS by 10–25% during these fly-by flights.

Under suitable wind conditions, the transport of pollutants from fossil fuel combustion (like cars and trucks from a nearby road) contaminated the data for short periods. The time periods with winds coming from the direction of the road, having high CO, nitric oxides (NO_x) and low single scattering albedo (ω_o) were assumed to be affected by cars and trucks; these data (<5% of the total data set) were removed and not considered in this study. Aerosol properties, for instance, σ_s, σ_a, AOT and PM2.5 averaged for 30 min intervals were used to derive the intensive optical properties like ω_o, mass scattering efficiency (α_s), mass absorption efficiency (α_a) and Ångström exponent (å). The dried size distribution of aerosols (D_p=10–414 nm) in the BL and FT was measured using a TSI scanning mobility particle sizer (SMPS model 3080). In some of the flights the size scans were made to smaller sizes only (D_p=346 nm). Since most of the smallest aerosols do not contribute significantly to the in light scattering, the always available size range from 42 up to 346 nm are used for calculating the scattering efficiency ($\Delta\sigma_s/\Delta CN$). The size scans were made over 2 min each. The next section describes the details of the methods and measurements used to derive the optical properties.

2.3 Aerosol optical properties

2.3.1 Aerosol light scattering

The light scattering properties of the dried aerosols were measured using two Radiance Research (RR, model M903) and one TSI (TSI, model 3563) nephelometers. The RR nephelometer measures σ_s at a single wavelength (545 nm) whereas the TSI nephelometer measures σ_s at three wavelengths (450, 550, 700 nm). The RR nephelometers were employed at the ground site (FNS) for simultaneous measurements of light scattering of dried and ambient aerosols. The TSI nephelometer was used for airborne observations. The calibrations of the nephelometers and the basic measurement strategy adopted herein have been described by Anderson and Ogren (1998). All the nephelometers used at the surface as well as in the airborne observations were calibrated during the field campaign using particle-free air and CO_2 as a

Table 3. Correlations of light scattering coefficient (σ_s) with CO and CN from the airborne (boundary layer-BL and free troposphere-FT 550 nm) and surface observations (545 nm) at FNS. The flights, shown by the respective numbers were conducted on the dates given in brackets in column 1. The correlation coefficients (r^2) of the slopes $\Delta\sigma_s/\Delta CN$ and $\Delta\sigma_s/\Delta CO$ are given in parenthesis.

Observations	Flight No [Date]	$(\Delta\sigma_s/\Delta CN)_{BL}$ (Mm^{-1} cm^{-3})	$(\Delta\sigma_s/\Delta CN)_{FT}$ (Mm^{-1} cm^{-3})	$(\Delta\sigma_s/\Delta CO)_{BL}$ (Mm^{-1} ppb^{-1})	$(\Delta\sigma_s/\Delta CO)_{FT}$ (Mm^{-1} ppb^{-1})
Airborne	04 [28 September]	0.011 (0.14)	0.12 (0.79)	0.36 (0.55)	1.02 (0.80)
	06 [30 September]	0.015 (0.64)	0.037 (0.76)	0.38 (0.67)	–
	07 [30 September]	0.018 (0.76)	0.026 (0.50)	0.38(0.67)	–
	08 [1 October]	0.019 (0.57)	0.033 (0.55)	0.38(0.67)	–
	24 [15 October]	0.019 (0.57)	0.076 (0.73)	0.40 (0.60)	1.50 (0.45)
Surface	16 Septmber–8 October	0.03 (0.30)	–	0.43 (0.88)	–

Table 4. Average Ångström exponent calculated from the airborne (nephelometer, å$_s$) and integrated (sunphotometer, å$_e$) observations. The wavelengths λ_1 and λ_2 used for computing the Ångström exponent from the nephelometer and the sunphotometer are 450–700 nm and 440–670 nm. In addition to the average å$_e$ during the airborne observation days, an average Ångström exponent is also calculated for the entire burning period. SD represents the standard deviation from the number of observations shown by the counts. Each count from airborne observations is 1 s whereas for the sunphotometer it is about 15 min.

Observations	Flight No (Date)	Ångström Exponent, å$_s$ (450–700 nm) Airborne nephelometer			Ångström Exponent, å$_e$ (440–670 nm) Sunphotometer		
		Avg.	SD	Counts	Avg.	SD	Counts
Individual days	– (21 September)	–	–	–	1.74	0.05	8
	– (25 September)	–	–	–	2.01	0.04	11
	– (5 October)	–	–	–	1.85	0.02	10
	04 (28 September)	1.90	0.33	10106	1. 70	0.05	11
	06 (30 September)	1.98	0.41	8103	1.57	0.04	7
	07 (30 September)	2.06	0.35	11149	1.57	0.04	7
	08 (1 October)	2.11	0.31	5269	1.40	0.13	13
	24 (15 October)	1.98	0.19	13166	1.53	0.06	3
Burning events	(16–27 September)	–	–	–	1.8	0.2	122

span gas. All the nephelometers were inter-compared by running them parallel to each other after the end of the airborne campaign. After including calibration factors, truncation correction and non-lambertian correction, good agreement was found (within 5%) in all the nephelometers at surface. Measurements of the total scattering coefficient in the RR and TSI nephelometers cover the angles 9–170° and 7–170°, respectively. The RR nephelometer data at FNS are corrected for the truncated angles using Mie calculations. The truncated angles (0–9°, 170–180°) contribute about 4% of the total light scattering by the dried fine aerosols (D$_p$<1.5 μm) in the biomass burning season. The truncation angles in the TSI nephelometer are slightly smaller (0–7°, 170–180°)

compared to the RR nephelometer. Based on the Mie calculations performed by us and Guyon et al. (2003c), the contribution by the truncated angles may be 4–16% of the total light scattering depending on the particle size distribution. However, due to unavailability of complete size distribution, σ_s is not corrected for truncation errors for the airborne observations using the TSI nephelometer. All the data from both the nephelometers (RR and TSI) presented in this article are converted to a standard temperature (25°C) and pressure (1000 hPa) using the method described by Anderson and Ogren (1998). The estimated combined accuracy of σ_s is <10%.

The spectral dependence of σ_s can be derived from the multi-wavelength (TSI nephelometer) measurements. This dependence is an intensive parameter in the sense that it depends on the aerosol size distribution and refractive index but, contrary to σ_s (at a wavelength λ) not on the aerosol concentration. It is generally assumed that the wavelength dependence of the scattering coefficient from the nephelometer can be described in the visible spectrum by an empirical equation as a power law of λ (Ångström, 1929):

$$\sigma_s(\lambda) = \beta_s \lambda^{-\mathring{a}_s} \tag{1}$$

where $\sigma_s(\lambda)$ is the scattering coefficient at wavelength λ, β_s is a constant, and $\mathring{a}_s$ is the non-dimensional Ångström exponent. In order to cover the widest possible spectral range, we compute $\mathring{a}_s$ from the nephelometer measurements at 450 nm and 700 nm to obtain $\mathring{a}_s$ i.e.,

$$\mathring{a}_s = -\frac{\log[\sigma_s(\lambda_1)/\sigma_s(\lambda_2)]}{\log(\lambda_1/\lambda_2)} \tag{2}$$

The variability in $\mathring{a}_s$ can be used to provide an insight on the types of aerosol from the nephelometer observations, since Mie theory shows that $\mathring{a}_s$ increases with decreasing aerosol particles size. For instance, $\mathring{a}_s$ values for fine anthropogenic aerosol encountered in polluted areas are typically larger than 1, whereas $\mathring{a}_s$ is low ($\sim$0.3) in regions dominated by coarse mode desert dust (Horvath and Trier, 1993; Eck et al., 1999). The mass scattering efficiency α_s is derived by normalizing the scattering coefficient σ_s with PM2.5 obtained from the TEOM.

2.3.2 Aerosol light absorption

The σ_a of aerosol particles was measured by a Particle Soot Absorption Photometer (PSAP) calibrated using a Photoacoustic spectrometer (PAS) as a reference. The PSAP measures σ_a based on the attenuation of light (565 nm) through a particle-loaded filter. Although Bond et al. (1999) have provided a calibration for the PSAP using laboratory-generated model aerosols and an optical extinction cell combined with an integrating nephelometer as reference, its validity for atmospheric aerosol is questionable, since the calibration is likely to depend on parameters such as aerosol size, single scattering albedo and RH (Weingartner et al., 2003, Arnott et al., 2003). In order to correct for potentially resulting systematic errors, we calibrated the PSAP in the field with a PAS (Arnott et al., 1999), which measures σ_a (532 nm) by converting the absorbed energy into an acoustic wave (Terhune and Anderson, 1977). In contrast to filter-based methods like the PSAP, the PAS measurement is performed on particles in their suspended state, i.e., sampling artefacts due to filter-particle interactions (Arnott et al., 2005) are avoided, and the PAS can be calibrated in the field using NO_2 as calibration gas (Arnott et al., 2000; Schmid et al., 2005). Laboratory studies with soot and biomass burning aerosols have shown good agreement between the PAS (accuracy 5%) and

an optical extinction cell (Schnaiter et al., 2005). To avoid potential complications in both PAS and PSAP due to elevated RH (Arnott et al., 2003), both the instruments were operated with dried aerosol ($RH<50\%$). The known PAS cross-sensitivity to NO_2 (Arnott et al. 2000) was corrected based on continuous NO_2 measurements with a NO_x analyzer (Trebs et al., 2006). For the PSAP calibration, the PAS and PSAP were operated in parallel for several days during the campaign as described in detail by Schmid et al. (2005). The calibration revealed that for relative humidity (RH) between 35% and 50% (inside the PSAP) the Bond-corrected PSAP overpredicted σ_a by about 18%. On the other hand, for some sampling periods with low RH (between 20% and 35%), as encountered during nighttime due to a higher drying efficiency of the nafion unit, the σ_a ratio of the PSAP (with Bond correction) and PAS decreased for unknown reasons from 1.18 to 0.65 possibly. Hence, the Bond correction, that is based on laboratory-generated nigrosin and ammonium sulfate aerosol, shows satisfactory agreement with the PSAP field calibrations except for some nighttime periods. After correcting for these systematic errors we assume the accuracy of σ_a measurements to be $<15\%$.

Analogous to α_s, the mass absorption efficiency (α_a) is computed by normalizing σ_a with the aerosol mass concentration obtained from PM2.5. Furthermore, the single scattering albedo (ω_o) is defined as

$$\omega_o = \frac{\sigma_s}{\sigma_s + \sigma_a} \tag{3}$$

Since the light scattering and absorption coefficients (i.e. σ_s, σ_a) were measured at 545 nm and 532 nm, respectively, we converted σ_a from 532 to 545 nm using a power law relationship as given in Eq. (1), where the absorption Ångström exponent was determined from the 450 and 615 nm channel of a multiple wavelengths Aethalometer (AE30, Magee Scientific) (Arnott et al., 2005), which was operated in parallel with a slightly larger inlet cutoff diameter than the PSAP (2.5 μm versus 1.5 μm) and under ambient conditions. Henceforth, σ_s, σ_a and ω_o will be presented at 545 nm. For the high pollution events, the absorption Ångström exponent reached values of about 2, which is close to what Kirchstetter et al. (2004) reported for biomass smoke particles from Africa.

Due to the elevated operating temperature in the TEOM (50°C), some of the organic matter have evaporated from aerosols. Simultaneous observations of TEOM and filter-based gravimetric mass indicate that the difference in gravimetrical and TEOM measurement of PM2.5 resulted in an underestimation of PM2.5 by 8%. This correction based on gravimetric method is applied in the PM2.5 data. This correction propagates in the σ_s and σ_a calculations.

2.3.3 Aerosol optical thickness

A sunphotometer (CIMEL, model CE 318-1) described by Holben et al. (1998) was set up on Abracos hill about 4 km

from the ground station FNS as a part of the AERONET network. The sunphotometer is used to measure column aerosol optical thickness (AOT) at 7 wavelengths (340, 380, 440, 500, 670, 870 and 1020 nm). The AOT data have been screened for cloud events according to a standardized procedure (Smirnov et al., 2000). The value of the AOT is indicative of the extinction of the solar radiation due to the columnar aerosol content and, similar to σ_s, the wavelength dependence of AOT can be expressed by a power law empirical equation (Ångström, 1929):

$$AOT(\lambda) = \beta_e \lambda^{-\mathring{a}_e} \qquad (4)$$

where

$$\mathring{a}_e = -\frac{\log[AOT(\lambda_1)/AOT(\lambda_2)]}{\log(\lambda_1/\lambda_2)} \qquad (5)$$

To calculate the Ångström exponent ($\mathring{a}_e$), we will be using the AOT at two wavelengths, 440 nm and 670 nm, which are very close to the $\mathring{a}_s$ wavelengths (450, 700 nm) measured by the nephelometer. The Ångström exponents from two independent methods ($\mathring{a}_s$, $\mathring{a}_e$) provide information on the aerosol size distribution averaged over height during the airborne observations as well as over the atmospheric column using the AOT measurements.

2.3.4 Excess ratios

Biomass burning emission information is usually represented in two basic forms: emission ratios or emission factors (Andreae and Merlet, 2001). These parameters relate the emission of a particular species of interest to that of a reference species, such as CO_2 to CO (for gases) and σ_s to CO (for aerosols-gases). To obtain "excess" concentrations, the ambient background concentrations must be subtracted from the values measured in the sample air. The method for calculation of the excess emission ratio (ER) is discussed in detail in Andreae and Merlet (2001) and in Le Canut et al. (1996), i.e.,

$$ER = \frac{\Delta y}{\Delta x} \qquad (6)$$

where $\Delta y / \Delta x$ is the average slope of correlation of species "y" with respect to "x" in a biomass burning environment (plume and/or haze mixed in the background air). The advantage of this method is that it is not necessary to estimate the background concentration of the species while computing the ER. Equation (6) is used to calculate the excess ratios of σ_s to CO, σ_s to CN, σ_s to PM2.5, and σ_a to PM2.5 for both the regional haze as well as smoke plumes.

3 Results and discussions

3.1 Measurements at the ground site FNS

Figure 2 shows the 30-min averaged time series of σ_s, σ_a, PM2.5 and CO for the burning season at FNS. A large
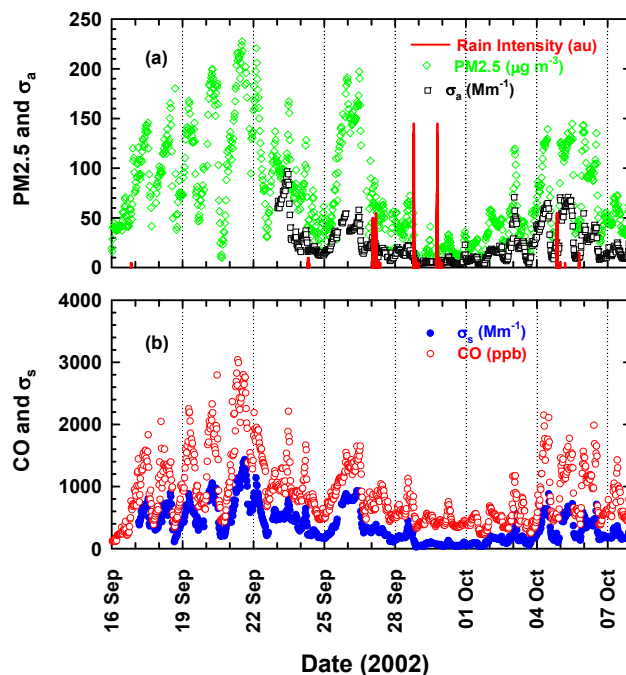

Fig. 2. Temporal variation of PM2.5 (diamonds), light absorption coefficient at 545 nm (σ_a, squares), light scattering coefficient at 545 nm (σ_s, solid circles) and CO mixing ratio (open circles) at 30 min intervals in the biomass burning season at the surface station (FNS). The rainfall (arbitrary units) is shown by the vertical bars.

variability up to 2 orders of magnitude is observed in σ_s, σ_a, PM2.5, and CO with values ranging 5–1435 Mm^{-1}, 1–70 Mm^{-1}, 2–225 $\mu g\,m^{-3}$, and 300–3500 ppb, respectively. The highest levels in σ_s, σ_a, PM2.5 and CO were observed during the heavily burning-influenced periods on 21, 25–26 September and 5 October (see Fig. 2). The lower values were typically observed after the rain events (e.g., 24 September, 27 September, 28 September–2 October). Some of the rainfall events, for instance on 28 September (vertical bars, Fig. 2), resulted in dramatic reduction of aerosol and CO concentrations. The simultaneous decrease in concentrations of aerosols and CO indicates that the clean-up was due to air mass replacement followed by fire suppression, while the role of scavenging was likely low. Since most of the period (16 September–8 October) is dominated by biomass burning aerosols (except for a few rain events), the aerosol properties along with CO are representative of biomass burning conditions.

Figure 3 shows the correlations of σ_s with PM2.5, CN, CO and also σ_a with PM2.5 at the pasture site FNS during the burning period. There are two populations of points in σ_a and σ_s. The number of points in the second population is less than 1% of total data, so correlations are dominating by the first population. The σ_s and σ_a of the aerosols are positively correlated with PM2.5, CN and CO. Good correlation
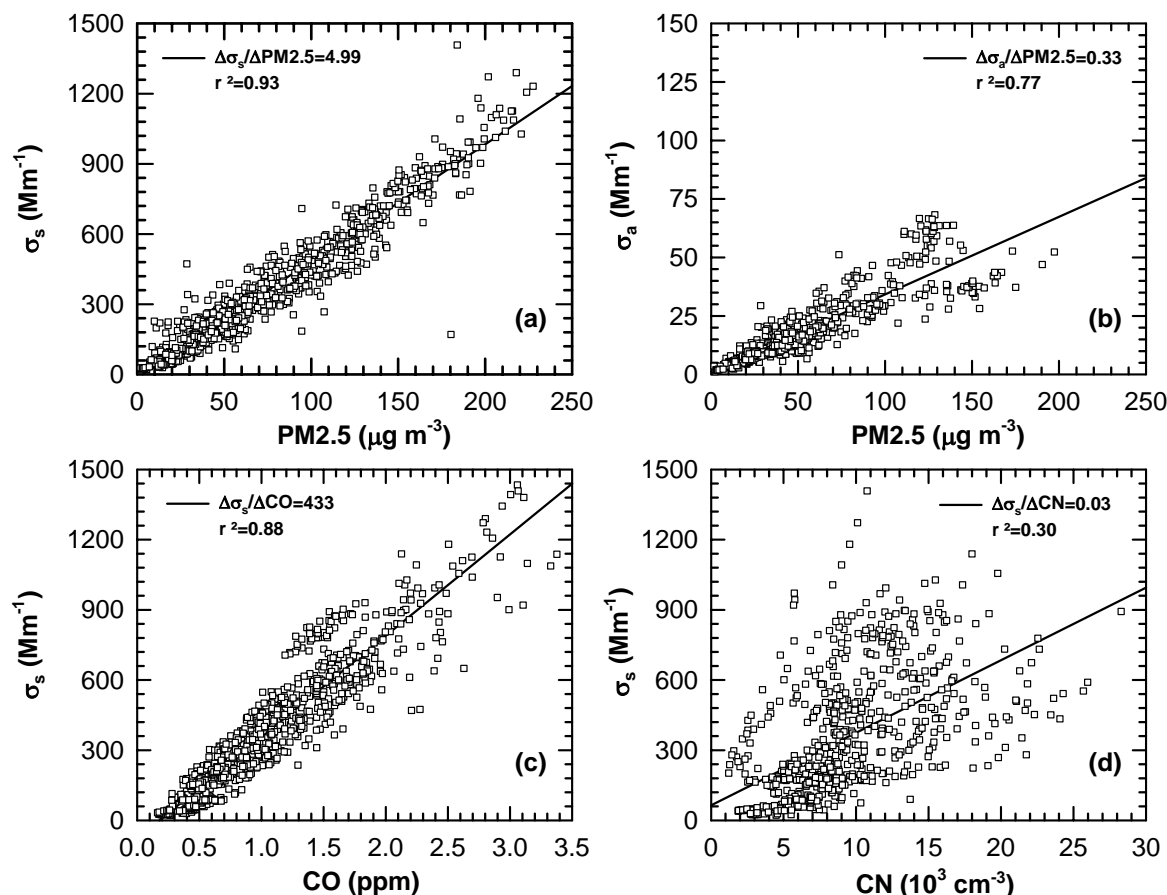
Fig. 3. Scatter plots and regression lines for 30-min averaged data of **(a)** light scattering coefficient (σ_s) at 545 nm versus aerosol mass concentration (PM2.5) at the ground station (FNS) during the biomass burning season. Similarly, **(b)** the light absorption coefficient (σ_a) at 545 nm versus PM2.5, **(c)** σ_s versus CO, and **(d)** σ_s versus aerosol number concentration (CN). The slopes are least-square-fitted lines. The corresponding correlation coefficients (r^2) of these parameters are shown on the respective plates.

is found between σ_s and PM2.5 (r^2=0.93) as well as between σ_s and CO (r^2=0.88). The correlation between σ_a and PM2.5 (r^2=0.70) is not as good as for σ_s and PM2.5. Poor correlation (r^2=0.30) is observed between σ_s and CN.

The average slopes of σ_s and σ_a with PM2.5 ($\Delta\sigma_s/\Delta$PM2.5, $\Delta\sigma_a/\Delta$PM2.5) are the average mass scattering efficiency (α_s) and mass absorption efficiency (α_a), 5.0 and 0.33 m^2 g^{-1}, respectively, during the burning period. The observed $\Delta\sigma_s/\Delta$CO is 0.433 Mm^{-1} ppb^{-1} (Fig. 3c). We note here that since the cut point (D$_p$) for the measurements of σ_s and σ_a is 1.5 μm, compared to PM2.5, our values are a lower estimate of the true α_s and α_a for these particles. The mass difference between PM1.5 and PM2.5 is less than 10% of PM2.5 during the dry season (Chand et al., 2006[2]).

The average ω_o for dried aerosols (*RH*=20–40%), calcu-

lated using Eq. (3), is about 0.92±0.02. This ω_o is consistent with the ω_o calculated from the AERONET data (0.92) obtained from the nearby site Abracos hill (4 km from FNS). Also, the observed ω_o is close to the earlier study conducted over the Amazon basin (Dubovik et al., 2002). At higher *RH* (>60%), the ω_o may be higher compared to the observed ω_o at drier conditions. The ω_o and other optical parameters showed pronounced diurnal variations, which will be discussed in detail in Chand et al. (2006)[2]. The hourly average values of ω_o at midnight (00:00 local time, LT) and midday (12:00 LT) are 0.91±0.02 and 0.94±0.02, respectively. The daytime aerosols are representative of a deeper boundary layer height (∼1600 m) than night time aerosols with a boundary layer height of about 200 m. Due to different mixing and transport times in the BL during day and night, the daytime aerosols are generally more aged than the aerosols in night time (Rissler et al., 2006). Observations of higher scattering efficiency for the aerosols at higher altitudes compared to those near ground (Sect. 3.2) corroborate our observation of higher ω_o during day time. The size distribution and Hygroscopic Tandem Differential Mobility Analyser (HTDMA)

---

[2] Chand, D., Schmid, O., Vestin, A., Artaxo, P., Frank, G. P., Guyon, P., Gatti, L. V., Swietlicki, E., and Andreae, M. O.: Diurnal variations in optical properties of aerosols at a pasture site over the Amazon Basin, in preparation, 2006.

observations show that the daytime aerosols have higher modal diameter compared to night time aerosols, most likely due to more aged aerosols being present in day time (Rissler et al., 2006; Chand et al., 2006[2]). The value of ω_o increases with increasing size (ageing) of aerosols. Under humid conditions, the ω_o is likely to increase even higher, when the ageing effect is taken into account together with the higher relative humidity.

Using CO as a conservative tracer of biomass burning (Andreae and Merlet, 2001), the good correlation between σ_s and CO indicates that most of the aerosols which contribute to σ_s have originated from biomass combustion. Also, good correlations of σ_s with PM2.5 and CO indicate that the scattering efficiency from the haze particles is relatively independent of the absolute pollution level during the burning period. The correlation between σ_s and CN is not good at FNS. The poor correlation coefficient between σ_s and CN is due to the large variability in the very small particles ($<$40 nm), which make a negligible contribution to light scattering. After excluding the aerosols below 40 nm, there is significant correlation ($r^2>0.60$) between σ_s and CN yielding a scattering efficiency of 0.016 Mm^{-1} per particle per cm^3 (Chand et al., 2006[2]).

The average mass scattering efficiency (α_s=5.0 m^2 g^{-1}) of the submicron dried aerosols observed in this study is consistent with the earlier observations during the LBA-EUSTACH 2 campaign in September–October 1999 over the Amazon Basin (Guyon et al., 2003b). However, the mass absorption efficiency (α_a=0.33 m^2 g^{-1}) in this study is about 10% higher than during the LBA-EUSTACH 2 campaign. The α_s and α_a of aged smoke aerosols over the tropical forest discussed by Reid et al. (2005a) are 4.1 m^2 g^{-1} and 0.5 m^2 g^{-1}, respectively. The airborne observations of relatively young aerosols during the "Smoke Clouds Aerosols and Radiation Brazil" (SCAR-B) campaign showed a lower α_s (2.8–3.6 m^2 g^{-1}) and higher α_a (0.7–1.1) over the Amazon Basin (Reid el., 1998a, b). The differences in observations of α_a in this study with the LBA-EUSTACH 2 and SCAR-B observations is likely due to different burning conditions, (flaming vs. smoldering), and higher particle concentrations leading to faster growth during aging processes.

3.2 Airborne measurements

The vertical structure and evolution of the aerosols from biomass burning can be assessed by measuring σ_s along with other parameters (e.g., CN, CO) at the surface and aloft in the BL and FT. For example, correlations of σ_s with CO at different altitudes can be used to get some insights on mixing/dilution of the aerosols when the air is transported from the BL to the FT. Similarly, correlations of σ_s with CN at different altitudes can be used to get some information on evolution/ageing (coagulation, condensation, etc.) of the aerosols when the air is transported from the BL to the FT.

Inter-comparison between the observations at FNS and on the aircraft was made using day time observations during the

seven fly-by flights at heights of 150–600 m above FNS. The ratios of the σ_s and CO from airborne observation are higher by (10–25%) during these fly-by flights. This could be attributed to the combined effects of higher CN, higher modal diameter of aerosols and lower CO at the upper heights. Figures 4a, c, e show scatter plots of σ_s with CN from the airborne observations. The flight tracks of the covered regions are shown in Fig. 1. The excess ratios ($\Delta\sigma_s/\Delta$CN) represent the scattering efficiency of aerosols during the vertical profiles covering BL and FT. Depending on the altitude and nature of the aerosols (haze or fresh plumes), the scattering efficiency ($\Delta\sigma_s/\Delta$CN) varies significantly, as shown in Table 3.

Similar to the variations at the ground site FNS, σ_s is positively correlated with CN in the BL as well as in the FT. However, unlike at FNS, the airborne observations show a better correlation between σ_s and CN. The aerosols during airborne observations show two populations during most of the flights. The transition between the two populations is at an altitude between 1200 and 2000 m. These modes, as shown by the slopes in Figs. 4a, b, c, e, and f, could be due to different ageing, size distributions and *RH* in the BL and FT. The good correlation (high r^2) in both modes indicates that most of the particles become optically active and contribute to light scattering when transported up from the surface to the BL and FT.

Figures 4b, d and f show the correlation of σ_s with CO from the airborne observations for flights 4, 6, 7, 8 and 24. A summary of $\Delta\sigma_s/\Delta$CO at 550 nm in the BL and FT is given in Table 3. Similar to the observations at the ground (FNS), the light scattering is positively correlated with CO in the BL with $\Delta\sigma_s/\Delta$CO in the range of 0.36–0.40 Mm^{-1} ppb^{-1}. This value from the airborne observations is close to the surface observations at FNS ($\Delta\sigma_s/\Delta$CO=0.42 Mm^{-1} ppb^{-1}). A good agreement in $\Delta\sigma_s/\Delta$CO between the ground and airborne observations in the BL covering a large area suggests that the biomass burning aerosol sampled at FNS reflects sources typical for the entire region, with similar emission characteristics as over the rest of the Amazon Basin (Table 3). Comparing the variations of σ_s with CN and CO in the BL and FT, the magnitude of vertical change is higher in $\Delta\sigma_s/\Delta$CN than in $\Delta\sigma_s/\Delta$CO (Table 3). The increase in $\Delta\sigma_s/\Delta$CN with height suggests a substantial reduction in the relative abundance of small, weakly scattering particles in the FT compared to the particles in the BL. The particles light scattering efficiency ($\Delta\sigma_s/\Delta$CN) increases 2–10 times from the surface to the FT, most probably due to the combined effects of coagulation and condensation when the air parcel get aged. In addition, the large scale meteorology may also play important role in deciding the $\Delta\sigma_s/\Delta$CN. Reid et al. (1998) has suggested a complicated effect of meteorology on optical properties of aerosols over the Amazon basin.
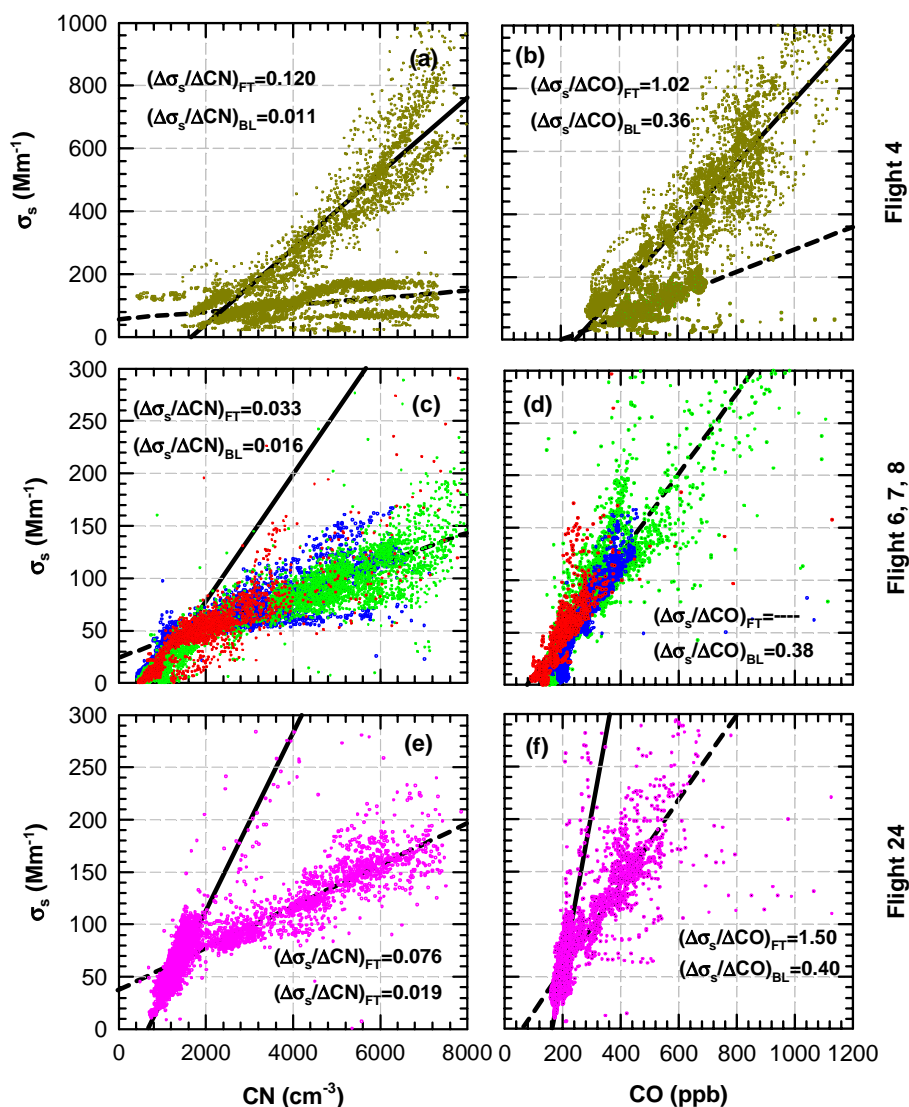
Fig. 4. Scatter plots and regression lines of the light scattering coefficient (σ_s) from the airborne observations at 550 nm against aerosol number concentration (CN) and CO for flight 4 **(a, b)**; flights 6, 7, 8 **(c, d)**; and flight 24 **(e, f)**. The slopes in the BL and FT are shown by the dashed and continuous lines, respectively.

The increase in $\Delta\sigma_s/\Delta$CN reflects in an analysis of particle volume as a function of altitude. Figure 5 shows the total volume normalized with numbers (V_n=ratio of total volume to the total number of aerosols) for the size range 42–346 nm (D_p) of dried aerosols as a function of height during flights 4, 6, 7, 8 and 24. The V_n increases with height showing maximum level at 2000–3000 m (700–800 hPa) during all the flights. The ratio of highest V_n in FT ($\sim$2500 m) to the lowest V_n in BL (500 m) varies from 1.3–1.6. Higher aerosol volume (V_n) aloft suggests that condensation of organic and possibly inorganic vapors as well as coagulation play important roles in changing the physical (size) properties of aerosol particles during ageing.

Some meteorological conditions (e.g., a strong BL inversion as observed on Flight 4 and 24), can increase the difference in $\Delta\sigma_s/\Delta$CN between the BL and FT. The strong inversion reduces the transport/mixing of air from the FT to the BL, and the ageing of the aerosols in the FT increases V_n and $\Delta\sigma_s/\Delta$CN. Assuming that σ_a per particle is independent of altitude during ageing, the increased $\Delta\sigma_s/\Delta$CN corresponds to an increase in ω_o up to 7% (from 0.92 to 0.98) for the aerosols in the FT. This assumption is corroborated by the lower ω_o during the night hours (0.91) for less aged aerosols and the higher ω_o in day time (0.94) for aged aerosols. More details on the diurnal variation in optical properties of aerosols at the surface site (FNS) over the
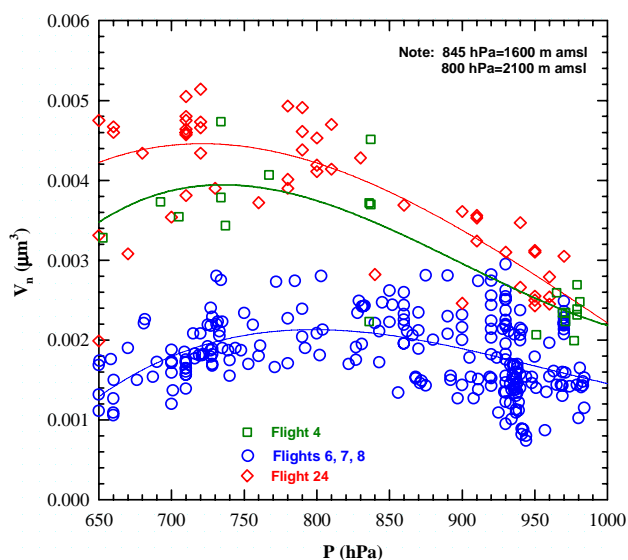
Fig. 5. Vertical variation in number-normalized total volume of aerosol (V_n) in the size range 42–346 nm (mobility, D_p) during the flights 4, 6, 7, 8 and 24. The curves are polynomial fits based on the least squared method.

Fig. 6. Scatter plot of light scattering coefficient (σ_s) with aerosol optical thickness (AOT) (both σ_s and AOT at 550 nm) during the biomass burning season (16 September–7 October). The AOT data are taken between 11:00 to 14:00 LT. The OSH and the correlation coefficient (r^2) also given in the figure.

Amazon Basin are being included in another manuscript under preparation (Chand et al., 2006[2]).

3.3 Vertically integrated measurements

In order to determine whether the characteristics of aerosols measured by sunphotometry at the ground agree with in-situ measurements in the atmospheric column (BL and FT), we compared the Ångström exponents derived from independent sunphotometer ($\mathring{a}_e$) and aircraft ($\mathring{a}_s$) measurements. A brief summary of $\mathring{a}_e$ and $\mathring{a}_s$ is given in Table 4. The mean airborne $\mathring{a}_s$ from the individual flights vary in the range of 1.9 to 2.1 whereas the column integrated $\mathring{a}_e$ varies in the range of 1.4 to 2.0. The mean values of $\mathring{a}_e$ and $\mathring{a}_s$ are 2.0±0.4 and 1.8±0.2, respectively. The small difference between $\mathring{a}_e$ and $\mathring{a}_s$ suggests that (1) the absorption coefficient is not as wavelength dependent as the scattering coefficient, leading to minimal effect of light absorption on the Ångström exponent, (2) the sunphotometer results at FNS are regionally representative, and that the aerosols in the FT above the ceiling height of the aircraft did not significantly influence the value of $\mathring{a}_e$.

Convective activity enhances the vertical mixing and transport of aerosols in the atmosphere during the dry/burning period. An indication of the vertical extent of the aerosol column during the burning dominated period can be provided by an aerosol index called "optical scale height" (OSH). OSH is defined as the height (in m) of a homogeneous aerosol column having the same extinction coefficient ($\sigma_{ext} = \sigma_s + \sigma_a$) as the one determined at ground level, and the same AOT as the one measured by the sunphotometer. A plate of AOT (550 nm) vs. σ_s at FNS (AOT is adjusted to the
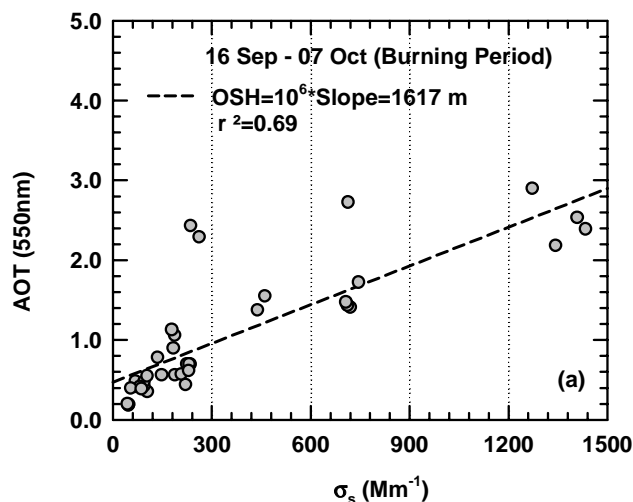
same wavelength as σ_s using Eqs. 4 and 5) yields a slope corresponding to an OSH of 1617 m (Fig. 6). The observed OSH is very close to the average height of the day time boundary layer (1600 m) during the burning season obtained by radiosonde measurements (G. Fisch, personal communication; Fisch et al., 2004). The OSH is consistent with the height (1200–2000 m) where the sharp transition is observed in $\Delta\sigma_s/\Delta CN$, as discussed in Sect. 3.2. Also, this is consistent with most of the optically active aerosols being confined to lower heights (i.e., the BL) during the burning period, as was also shown by Andreae et al. (2004; see their Fig. 2). Haze layers at higher elevations were commonly observed during the aircraft flights, but were optically much thinner than the CBL aerosol layer. This is further supported by the vertical profiles of CN and σ_s (Fig. 7). Due to large horizontal coverage and sampling of cleaner air (background) and smoke plumes, there is large vertical variability in both σ_s and CN. However, as an average, most of the optically active aerosols are below 2000 m (Fig. 7). This is consistent with the OSH, as shown by Fig. 6.

4 Summary and conclusions

Detailed ground and airborne measurements were taken over the Amazon Basin during the LBA-SMOCC experiment conducted during the dry season (September–October, 2002). These results have shed light on the optical and physical properties of biomass burning aerosols. The relationships between observations at the ground and in the BL and FT have been investigated.
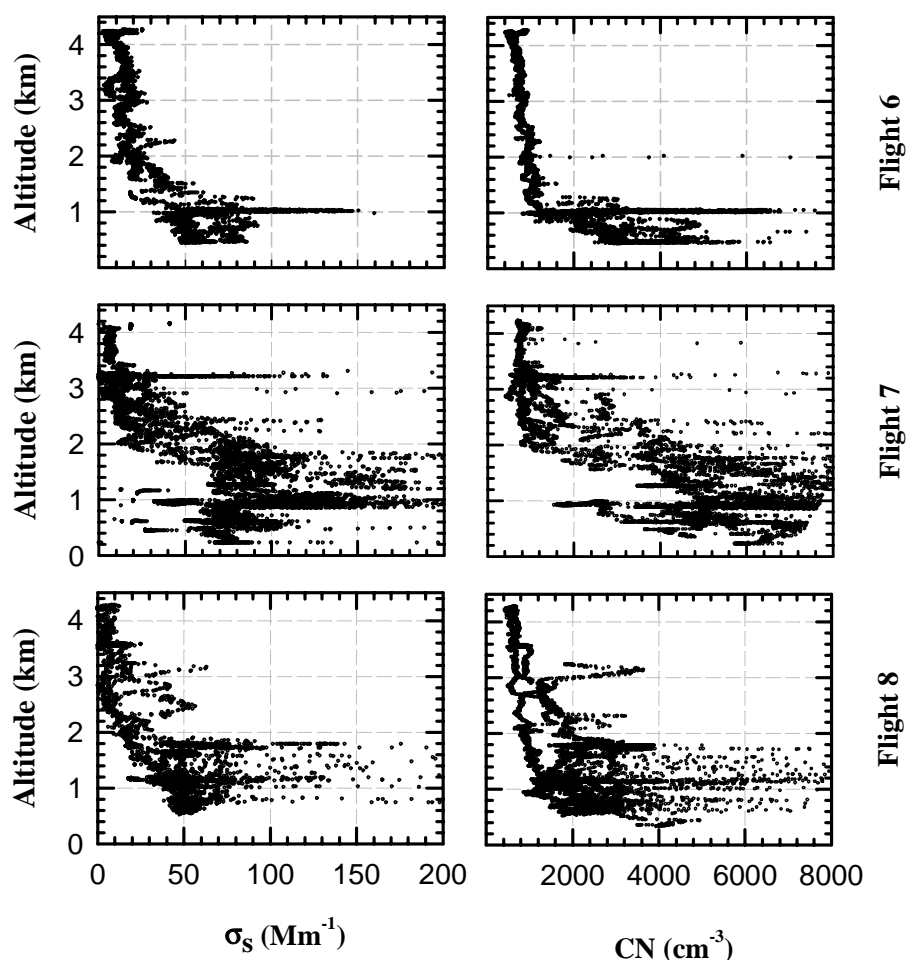
Fig. 7. Vertical variations in light scattering coefficient (σ_s 550 nm) and aerosol number density (CN) from the airborne observations (flights 6, 7 and 8) during the biomass burning season (September–October) over the Amazon Basin.

In general, all the aerosol extensive properties and CO showed large variability during the biomass burning season. During some of the most intensive burning periods, very high mass loading (PM2.5>225 μg m^{-3}) resulted in scattering coefficients as high as 1435 Mm^{-1} at 545 nm. At the same time, the aerosol optical depth at 500 nm reached values of more than 3 and CO exceeded 3000 ppb. A few rain events reduced the aerosol loadings and optical effects by two orders of magnitude.

The mass scattering and absorption efficiencies, α_s and α_a, relative to PM2.5 dried aerosols at about 545 nm at/near the ground are found to be 5.0 and 0.33 m^2 g^{-1}, respectively. The observed ω_o of dried aerosols at 545 nm is 0.92±0.02. The $\Delta\sigma_s/\Delta$CN in the free troposphere (between 1600 to 4200 m a.m.s.l.) is about 1.6 to 10.9 times higher than in the BL (below 1600 m a.m.s.l.). Assuming the same absorption efficiency of aerosols with altitude, this increase of σ_s in the FT can increase ω_o up to 7% from 0.92 to 0.98.

The Ångström exponent (2.0±0.4) computed from the airborne observations below 4200 m is close to the Ångström exponent (1.8±0.2) calculated by column integrated (sunphotometer) measurements. This suggests that (1) the absorption coefficient σ_a is not as wavelength dependent as the scattering coefficient σ_s, leading to minimal effect of light absorption on the Ångström exponent and, (2) the sunphotometer results at FNS are regionally representative, and (3) the aerosols in the FT above the ceiling height (4200 m) of the aircraft do not significantly influence the value of column-integrated Ångström exponent å$_e$.

The strong correlation of σ_s with PM2.5 and CO indicates that (1) most of the aerosol mass has originated from biomass combustion and (2) the smoke-laden air with different CO and mass loading has similar source (same α_s) and emission characteristics. The σ_s does not correlate well with the aerosol number concentration (CN) at the ground, however, it has a better correlation aloft in the BL and FT. This indicates that the ageing process plays an important role in the optical and physical properties of aerosols.

The correlation analysis between σ_s and aerosol AOT suggests that most of the aerosols are confined to the lower levels of the atmosphere (<1617 m) during the burning season. This is consistent with the vertical variability of σ_s and CN. Similar levels of $\Delta\sigma_s/\Delta CO$ at surface site and airborne observations covering a large area in the BL again suggest that the burning activities over the Amazon Basin have similar sources and fuel emission characteristics. Larger variation in σ_s with CN than with CO suggest that condensation-coagulation plays an important role in changing the radiative properties of aerosols. The scattering efficiency of aerosols (V_n) increases with height, having a maximum at 1700–3000 m.

This is the first study presenting a comprehensive data set on optical properties of aerosols at the ground, BL and FT in the dry season over the Amazon Basin. This data set, along with the data from the SCAR-B and LBA-EUSTACH2 campaigns, can be used to validate the optical parameters retrieved from satellites. The combined ground, airborne and remote sensing observations can be valuable to assess the role of biomass burning and its impact at local, regional and global scales.

Edited by: D. Rosenfeld

References

Andreae, M. O., Browell, E. V., Garstang, M., Gregory, G. L., Harriss, R. C., Hill, G. F., Jacob, D. J., Pereira, M. C., Sachse, G. W., Setzer, A. W., Dias, P. L. S., Talbot, R. W., Torres, A. L., and Wofsy, S. C.: Biomass-burning emissions and associated haze layers over Amazonia, J. Geophys. Res.-Atmos., 93, 1509–1527, 1988.

Andreae, M. O. and Crutzen, P. J.: Atmospheric aerosols: Biogeochemical sources and role in atmospheric chemistry, Science, 276, 1052–1058, 1997.

Andreae, M. O. and Merlet, P.: Emission of trace gases and aerosols from biomass burning, Global Biogeochem. Cycles, 15(4), 955–966, 2001.

Andreae, M. O., Artaxo, P., Brandao, C., Carswell, F. E., Ciccioli, P., da Costa, A. L., Culf, A. D., Esteves, J. L., Gash, J. H. C., Grace, J., Kabat, P., Lelieveld, J., Malhi, Y., Manzi, A. O., Meixner, F. X., Nobre, A. D., Nobre, C., Ruivo, M., Silva-Dias, M. A., Stefani, P., Valentini, R., von Jouanne, J., and Waterloo, M. J.: Biogeochemical cycling of carbon, water, energy, trace gases, and aerosols in Amazonia: The LBA-EUSTACH experiments, J. Geophys. Res.-Atmos., 107(D20), 8066, doi:10.1029/2001JD000524, 2002.

Andreae, M. O., Rosenfeld, D., Artaxo, P., Costa, A. A., Frank, G. P., Longo, K. M., and Silva-Dias, M. A. F.: Smoking Rain Clouds over the Amazon, Science, 303, 1337–1342, 2004.

Anderson, T. L. and Ogren, J. A.: Determining aerosol radiative properties using the TSI 3563 integrating nephelometer, Aerosol Sci. Technol., 29, 57–69, 1998.

Ångström, A.: On the atmospheric transmission of Sun radiation and on dust in the air, Geogr. Ann., 12, 130–159, 1929.

Artaxo, P., Fernandes, E. T., Martins, J. V., Yamasoe, M. A., Hobbs, P. V., Maenhaut, W., Longo, K. M., and Castanho, A.: Large Scale Aerosol Source Apportionment in Amazonia, J. Geophys. Res., 103(D24), 31 837–31 848, 1998.

Artaxo, P.: The atmospheric component of biogeochemical cycles in the Amazon basin, in: The biogeochemistry of the Amazon basin, edited by: McClain, M. E., Victória, R., Richey, J. E., Oxford University Press, 42–52, 2001.

Artaxo, P., Martins, J. V., Yamasoe, M. A., Procópio, A. S., Pauliquevis, T. M., Andreae, M. O., Guyon, P., Gatti, L. V., and Leal, A. M. C.: Physical and chemical properties of aerosols in the wet and dry seasons in Rondônia, Amazonia, J. Geophys. Res.-Atmos., 107(D20), 8081, doi:10.1029/2001JD000666, 2002.

Arnott, W. P., Moosmüller, H., Rogers, C. F., Jin, T., and Bruch, R.: Photoacoustic spectrometer for measuring light absorption by aerosols: Instrument description, Atmos. Environ., 33, 2845–2852, 1999.

Arnott, W. P., Moosmüller, H., and Walker, J. W.: Nitrogen dioxide and kerosene-flame soot calibration of photoacoustic instruments for measurement of light absorption by aerosols, Rev. Sci. Instrum., 71, 4545–4552, 2000.

Arnott, W. P., Moosmüller, H., Sheridan, P. J., Ogren, J. A., Raspet, R., Slaton, W. V., Hand, J. L., Kreidenweis, S. M., and Collett Jr., J. L.: Photoacoustic and filter-based ambient aerosol light absorption measurements: Instrument comparisons and the role of relative humidity, J. Geophys. Res.-Atmos., 108(D1), 4034, doi:10.1029/2002JD002165, 2003.

Arnott, W. P., Khadeejeh, H., Moosmüller, H., Sheridan, P. J., and Ogren, J. A.: Towards aerosol light-absorption measurements with a 7-wavelength aethalometer: Evaluation with a photoacoustic instrument and 3-wavelength nephelometer, Aerosol Sci. Technol., 39, 17–29, 2005.

Bond, T. C., Anderson, T. L., and Campbell, D.: Calibration and intercomparison of filter-based measurements of visible light absorption by aerosols, Aerosol Sci. Technol., 30(6), 582–600, 1999.

Charlson, R. J., Schwartz, S. E., Hales, J. M., Cess, R. D., Coakley, J. A., Hansen, J. E., and Hoffman, D. J.: Climate forcing by anthropogenic aerosols, Science, 255, 423–430, 1992.

Crutzen, P. J. and Andreae, M. O.: Biomass burning in the tropics: Impact on atmospheric chemistry and biogeochemical cycles, Science, 250, 1669–1678, 1990.

Eck, T. F., Holben, B. N., Slutsker, I., and Setzer, A.: Measure-

ments of irradiance attenuation and estimation of aerosol single scattering albedo for biomass burning aerosols in Amazonia, J. Geophys. Res.-Atmos., 103, 31 865–31 878, 1998.

Eck, T. F., Holben, B. N., Reid, J. S., Dubovik, O., Smirnov, A., O'Neill, N. T., Slutsker, I.,. and Kinne, S.: The wavelength dependence of the optical depth of biomass burning, urban and desert dust aerosols, J. Geophys. Res., 104, 31 333–31 350, 1999.

Eck, T. F., Holben, B. N., Reid, J. S., O'Neill, N. T., Schafer, J. S., Dubovik, O., Smirnov, A., Yamasoe, M. A., and Artaxo, P.: High aerosol optical depth biomass burning events: A comparison of optical properties for different source regions, Gepohys. Res. Lett., 30(20), 2035, doi:10.1029/2003GL017861, 2003.

Fisch, G., Tota, J., Machado, L. A. T., Silva Dias, M. A. F., Lyra, R. F. da F., Nobre, C. A., Dolman, A. J., and Gash, J. H. C.: The convective boundary layer over pasture and forest in Amazonia, Theor. Appl. Climatol., doi:10.1007/s00704-004-0043-x, 78, 47–59, 2004.

Gash, J. H. C., Nobre, C. A., Roberts, J. M., and Victoria, R. L.: Amazonian deforestation and climate, John Wiley & Sons Ltd, Chichester, England, 1996.

Guyon, P., Boucher, O., Graham, B., Beck, J., Mayol-Bracero, O. L., Roberts, G. C., Maenhaut, W., Artaxo, P., and Andreae, M. O.: Refractive index of aerosol particles over the Amazon tropical forest during LBA-EUSTACH 1999, J. Aerosol Sci., 34(7), 883–907, 2003a.

Guyon, P., Graham, B., Roberts, G. C., Mayol-Bracero, O. L., Maenhaut, W., Artaxo, P., and Andreae, M. O.: In-canopy gradients, composition, sources, and optical properties of aerosol over the Amazon forest, J. Geophys. Res.-Atmos., 108(D18), 4591, doi:10.1029/2003JD003465, 2003b.

Guyon, P., Graham, B., Beck, J., Boucher, O., Gerasopoulos, E., Mayol-Bracero, O. L., Roberts, G. C., Artaxo, P., and Andreae, M. O.: Physical properties and concentration of aerosol particles over the Amazon tropical forest during background and biomass burning conditions, Atmos. Chem. Phys., 3, 951–967, 2003c.

Guyon, P., Graham, B., Roberts, G. C., Mayol-Bracero, O. L., Maenhaut, W., Artaxo, P., and Andreae, M. O.: Sources of optically active aerosol particles over the Amazon forest, Atmos. Environ., 38, 1039–1051, 2004.

Guyon, P., Frank, G., Welling, M., Chand, D., Artaxo, P., Rizzo, L., Nishioka, G., Kolle, O., Fritsch, H., Silva Dias, M. A. F., Gatti, L. V., Cordova, M., and Andreae, M. O.: Airborne measurements of trace gas and aerosol particle emissions from biomass burning in Amazonia, Atmos. Chem. Phys., 2989–3002, 2005.

Hobbs, P. V., Reid, J. S., Kotchenruther, R. A., Ferek, R. J., and Weiss, R.: Direct radiative forcing by smoke from biomass burning, Science, 275, 1776–1778, 1997.

Hobbs, P. V., Sinha, P., Yokelson, R. J., Christian, T. J., Blake, D. R., Gao, S., Kirchstetter, T. W., Novakov, T., and Pilewskie, P.: Evolution of gases and particles from a savanna fire in South Africa, J. Geophys. Res.-Atmos., 108(D13), 8485, doi:10.1029/2002JD002352, 2003.

Holben, B. N., Eck, T. F., Slutsker, I., Tanré, D., et al.: AERONET – A federated instrument network and data archive for aerosol characterization, Remote Sens. Environ., 66, 1–16, 1998.

Horvath, H. and Trier, A.: A study of the aerosol of Santiago de ChileFII: mass extinction coefficients, visibilities and Angstrom exponents, Atmos. Environ., 27A(3), 385–395, 1993.

Intergovernmental Panel on Climate Change (IPCC): Third Assess-

ment Report, Climate Change 2001: The Scientific Basis, edited by: Houghton, J. T., Cambridge Univ. Press, New York, 2001.

Kirchstetter, T. W., Novakov, T., and Hobbs, P. V.: Evidence that the spectral dependence of light absorption by aerosols is affected by organic carbon, J. Geophys. Res.-Atmos., 109, D21 208, doi:10.1029/2004JD004999, 2004.

Kirkman, G. A., Gut, A., Ammann, C., Gatti, L. V., Cordova, A. M., Moura, M. A. L., Andreae, M. O., and Meixner, F. X.: Surface exchange of nitric oxide, nitrogen dioxide, and ozone at a cattle pasture in Rondônia, Brazil, J. Geophys. Res.-Atmos., 107(D20), 8083, doi:10.1029/2001JD000523, 2002.

Kotchenruther, R. A. and Hobbs, P. V.: Humidification factors of aerosols from biomass burning in Brazil, J. Geophys. Res.-Atmos., 103, 32 081–32 089, 1998.

Le Canut, P., Andreae, M. O., Harris, G. W., Wienhold, F. G., and Zenker, T.: Airborne studies of emissions from savanna fires in southern Africa. 1. Aerosol emissions measured with a laser optical particle counter, J. Geophys. Res.-Atmos., 101(D19), 23 615–23 630, 1996.

Martins, J. V., Artaxo, P., Liousse, C., Reid, J. S., Hobbs, P. V., and Kaufman, Y. J.: Effects of black carbon content, particle size and mixing on light absorption by aerosol particles from biomass burning in Brazil, J. Geophys. Res.-Atmos., 103, 32 041–32 050, 1998.

Procopio, A. S., Remer, L. A., Artaxo, P., Kaufman, Y. J., and Holben, B. N.: Modeled spectral optical properties for smoke aerosols in Amazonia, Geophys. Res. Lett., 30(24), 2265–2270, doi:10.1029/2003GL018063, 2003.

Procópio, A. S., Artaxo, P., Kaufman, Y. J., Remer, L. A., Schafer, J. S., and Holben, B. N.: Multiyear analysis of Amazonian biomass burning smoke radiative forcing of climate, Geophys. Res. Lett., 31(3), L03108–L03112, doi:10.1029/2003GL018646, 2004.

Ramanathan, V., Crutzen, P. J., Kiehl, J. T., and Rosenfeld, D.: Aerosols, climate and the hydrological cycle, Science, 294, 2119–2124, 2001.

Reid, J. S. and Hobbs, P. V.: Physical and chemical properties of individual biomass fires in Brazil, J. Geophys. Res.-Atmos., 103, 32 013–32 030, 1998.

Reid, J. S., Hobbs, P. V., Ferek, R. J., Blake, D. R., Martins, J. V., Dunlap, M. R., and Liousse, C.: Physical, chemical, and optical properties of regional hazes dominated by smoke in Brazil, J. Geophys. Res.-Atmos., 103, 32 059–32 080, 1998.

Reid, J. S., Eck, T. F., Christopher, S. A., Koppmann, R., Dubovik, O., Eleuterio, D. P., Holben, B. N., Reid, E. A., and Zhang, J.: A review of biomass burning emissions part III: intensive optical properties of biomass burning particles, Atmos. Chem. Phys., 5, 827–849, 2005a.

Reid, J. S., Koppmann, R., Eck, T. F., and Eleuterio, D. P.: A review of biomass burning emissions, part II: Intensive physical properties of biomass burning particles, Atmos. Chem. Phys., 5, 799–825, 2005b.

Rissler, J., Vestin, A., Swietlicki, E., Fisch, G., Zhou, J., Artaxo, P., and Andreae, M. O.: Size distribution and hygroscopic properties of aerosol particles from dry-season biomass burning in Amazonia, Atmos. Chem. Phys., 6, 471–491, 2006, http://www.atmos-chem-phys.net/6/471/2006/.

Rosenfeld, D.: Suppression of rain and snow by urban and industrial air pollution, Science, 287, 1793–1796, 2000.

Ross, J. L., Hobbs, P. V., and Holben, B.: Radiative characteristics

of regional hazes dominated by smoke from biomass burning in Brazil: Closure tests and direct radiative forcing, J. Geophys. Res.-Atmos., 103, 31 925–31 941, 1998.

Satheesh, S. K. and Ramanathan, V.: Large differences in the tropical aerosol forcing at the top of the atmosphere and Earth's surface, Nature, 405, 60–63, 2000.

Schmid, O., Artaxo, P., Arnott, W. P., Chand, D., Gatti, V. L., Frank, G. P., Hoffer, A., Schnaiter, M., and Andreae, M. O.: Spectral light absorption by ambient aerosols influenced by biomass burning in the Amazon Basin – I. Comparison and field calibration of absorption measurement techniques, Atmos. Chem. Pyhs. Discuss., 5, 9355–9404, 2005.

Schnaiter, M., Schmid, O., Petzold, A., Fritzsche, L., Klein, K.-F., Andreae, M. O., Helas, G., Thielmann, A., Grimmler, M., Möhler, O., Linke, C., and Schurath, U.: Measurement of wavelength-resolved light absorption by aerosols utilizing a UV-VIS extinction cell, Aerosol Sci. Technol., 39, 249–260, 2005.

Smirnov, A., Holben, B. N., Eck, T. F., Dubovik, O., and Slutsker, I.: Cloud screening and quality control algorithms for the AERONET data base, Remote Sens. Environ., 73, 337–349, 2000.

Terhune, R. W. and Anderson, J. E.: Spectrophone measurements of the absorption of visible light by aerosols in the atmosphere, Optics Letters, 1, 70–72, 1977.

Trebs, I., Meixner, F. X., Slanina, J., Oties, R. P., Jongejan, P., and Andreae, M. O.: Real-time measurements of ammonia, acidic trace gases and water-soluble inorganic aerosol species at a rural site in the Amazon Basin, Atmos. Chem. Phys., 4, 967–987, 2004,
http://www.atmos-chem-phys.net/4/967/2004/.

Trebs, I., Lara, L. B. L. S., Zeri, L. M. M., Gatti, L. V., Artaxo, P., Dlugi, R., Slanina, J., Andreae, M. O., and Meixner, F. X.: Dry and wet deposition of inorganic nitrogen compounds to a tropical pasture site (Rondônia, Brazil), Atmos. Chem. Phys., 6, 447–469, 2006,
http://www.atmos-chem-phys.net/6/447/2006/.

Weingartner, E., Saathoff, H., Schnaiter, M., Streit, N., Bitnar, B., and Baltensperger, U.: Absorption of light by soot particles: determination of the absorption coefficient by means of aethalometer, J. Aerosol Sci., 34, 1445–1463, 2003.